OPTICAL REVIEW Vol. 13, No. 6 (2006) 436–442

Resolving Discrepancy between Theoretical and Experimental Optical Trapping Forces Using Effects of Beam Waist and Trapping Position Displacement due to Gravity

Hiroo UKITA*, Takashi SAITOH† and Noboru SAKAHARA‡

Faculty of Science and Engineering, Ritsumeikan University, 1-1-1 Nojihigashi, Kusatsu, Shiga 525-8677, Japan

(Received June 5, 2006; Accepted September 7, 2006)

Optical trapping forces of polystyrene microspheres are analyzed both theoretically and experimentally, and comparisons are made between the two. Discrepancies are mainly caused by straight-ray approximation for axial trapping, and by trapping-position vertical displacement due to gravity for transverse trapping.

Key words: optical tweezers, optical trapping force, trapping position, microsphere, straight ray, parabolic ray, beam waist, axial trapping, transverse trapping

1. Introduction

Optical tweezers are a promising tool to manipulate,[1,2] align,[3,4] fabricate,[5,6] and rotate[7,8] microobjects. A single-beam gradient-force optical trap has been applied experimentally in various scientific and engineering fields including biology,[9,10] microchemistry,[11] physics,[12] and micromechanics.[13] Moreover, there is also a great deal of theoretical knowledge in this field. Nevertheless, quantitative comparisons between theoretical and experimental analyses have not yet been fully performed.

In this study, basic optical trapping characteristics for microspheres are analyzed both theoretically and experimentally, and comparisons between the two are examined. In theoretical analysis, both straight[14] and parabolic ray optics models are used to calculate trapping forces by considering Brownian movement. In experimental analysis,[15] particles are trapped with both upward- and downward-directed yttrium–aluminum–garnet (YAG) laser beams,[16] and minimum laser powers for both axially and transversally trapped particles are measured. Microspheres used for the experiment are 3.23-, 5.85-, 7.73-, 10-, 20-, 30-, 40-, and 50-μm-diameter polystyrene. The density is 1.06 g/cm^3 and the index of refraction is 1.60.

When a comparison of the trapping forces obtained theoretically and experimentally is made, discrepancy between the two is due to both axial and lateral trappings. The former discrepancy was resolved by considering a parabolic ray due to the beam waist instead of a straight ray, and the latter discrepancy was resolved by considering the trapping efficiency decrease due to the trapping (focal) position displacement caused by the gravitational force.

2. Theoretical Analysis

Trapping efficiency largely depends on the angle of incident ray, and the maximum trapping efficiency is obtained at the angle of about 70° for a polystyrene sphere in water. Therefore, the numerical aperture (NA) of the objective lens corresponding to the angle arcsin (NA/n_1) is greater than 1.2, which results in the tight convergence of the laser beam, where n_1 is the refractive index of the medium (water).

In general, the following steps are taken for optical trapping force/efficiency calculations.

1. Decompose the beam into individual rays with appropriate intensity and direction.
2. Trace each individual ray.
3. Find θ_1, the angle of incidence to the microsphere, of a ray entering the objective lens aperture at an arbitrary point (r, β).
4. Compute the Fresnel transmission T and reflection R coefficients at the incident point.
5. Compute the scattering trapping efficiency Q_s and gradient trapping efficiency Q_g for that ray (see appendix A).
6. Integrate the contribution of all rays within the convergent angle.
7. Compute the total trapping efficiency using $Q_t = \sqrt{Q_s^2 + Q_g^2}$.

As shown above, a trapping force is obtained by the vector sum of the contributions of all rays within the convergence angle. This trapping force varies according to the focus of the laser beam. The axial trapping efficiency is defined when the focus is on the centerline of the microsphere parallel to the optical axis, as shown in Fig. 1(a). The transverse trapping efficiency is defined when the focus is on the centerline of the microsphere perpendicular to the optical axis, as shown in Fig. 1(b). Conventional on-axis trapping analyses, i.e., the trapping position is on the axis in both cases, are shown in §2.1 and §2.2, while off-axis trapping analysis is shown in §2.3.

2.1 Straight-ray model

In the analysis decomposed rays with appropriate intensity and direction propagate in straight lines. Figure 1 shows the total trapping efficiency Q_t exerted on a polystyrene sphere

*E-mail address: ukita@se.ritsumei.ac.jp
†Currently with NEC, Kawasaki 210-0012, Japan.
‡Currently with NEC, Kashiwa, Chiba 277-0841, Japan.

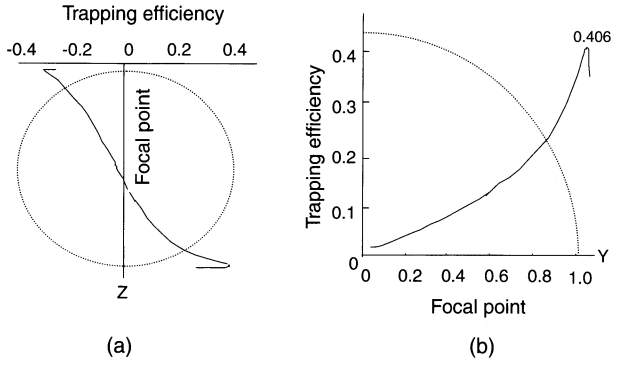

Fig. 1. Total trapping efficiency exerted on polystyrene microsphere suspended in water by trap with uniformly filled input aperture of NA = 1.25 (a) for axial and (b) for transversal directions.

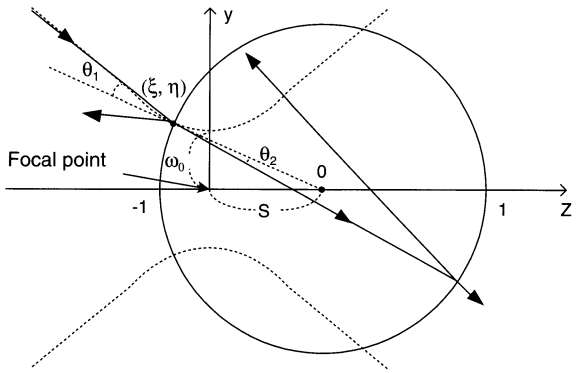

Fig. 2. Geometry for calculating exact axial trapping efficiency for microsphere considering beam waist.

suspended in water by a trap with a uniformly filled input aperture of NA = 1.25 which is focused along the optical axis at positions $+s$ and $-s$ below the center of the sphere, (a) shows the total trapping efficiency for the axial trap and (b) that for the transverse trap. Both show a maximum when the focus (trapping position) is near the surface of the sphere and decrease as the focus approaches the center of the sphere. At these surface positions, the laser power for trapping becomes minimum. We can also find that the upward-directed beam is more effective in trapping the microsphere than the downward-directed beam because the scattering force is added to the gradient force for the former.[16)]

2.2 *Parabolic-ray model*

Under actual conditions, the focused light beam has a beam waist, which means that each ray varies its direction near the focus. Therefore, the angle of incidence θ_1 varies from that of the straight line, resulting in the necessary recalculation of the exact optical pressure force. Instead of using straight-ray optics, we introduce a parabolic (Gaussian) beam profile (1) of a beam waist ω_0 and depth of focus Z_0 as

$$\omega_0 = \frac{\lambda}{2\mathrm{NA}}, \quad Z_0 = k\omega_0^2, \tag{1}$$

where k is the wave number $2\pi/\lambda$, λ is the wavelength, and NA is the numerical aperture of the objective lens.

When a Gaussian ray passing at $r = r$ in the aperture of the objective lens enters the sphere at the point (ξ, η) on the sphere surface, as shown in Fig. 2, the coordinates (ξ, η) are expressed as

$$\xi = \frac{2sZ_0^2 - \sqrt{4s^2Z_0^2 - 4Z_0^2\left[s^2 - r_0^2 + \left(\frac{r}{R_\mathrm{m}}\right)^2\omega_0^2\right]\left[Z_0^2 + \left(\frac{r}{R_\mathrm{m}}\right)^2\omega_0^2\right]}}{2\left[Z_0^2 + \left(\frac{r}{R_\mathrm{m}}\right)^2\omega_0^2\right]} \tag{2}$$

$$\eta = \sqrt{r_0^2 - (s - \xi)^2}, \tag{3}$$

where, s is the distance from the center of the microsphere and R_m is the maximum value of r. Then, the angle of incidence $\theta_1(r)$ is calculated from eq. (4) as the angle between the tangent vector $\boldsymbol{a}$ of the Gaussian ray at (ξ, η) and the direction vector $\boldsymbol{b}$ pointing to the center of the sphere.

$$\theta_1 = \arccos\frac{\boldsymbol{ab}}{|\boldsymbol{a}| \cdot |\boldsymbol{b}|} \tag{4}$$

After the angle of incidence $\theta_1(r)$ is defined, the trapping efficiencies $Q_\mathrm{s}(\xi, \eta)$ and $Q_\mathrm{g}(\xi, \eta)$ of a ray hitting the intersection (ξ, η) can be obtained using eqs. (A·1) and (A·2).

Figure 3 shows the results for a polystyrene sphere suspended in water. Considering the beam waist, it is seen from the figure that the axial trapping efficiency decreases to 50% that of the straight lines. This is caused by the fact that focused rays are almost parallel to the optical axis near the focus, as shown in the upper left sketch in the figure. On the other hand, for the transverse trapping efficiency along the axis perpendicular to the optical axis, both straight and parabolic beam rays have almost the same numerical results. This is based on the fact that the angles of incidence at the surface of the sphere are almost equal for both approximations, because the laser focus is located on the centerline (not near the surface) of the sphere.

2.3 *Off-axis trapping efficiency analysis*

In this off-axis analysis, decomposed rays propagate in straight lines, as shown in Fig. 4, for simplicity and the

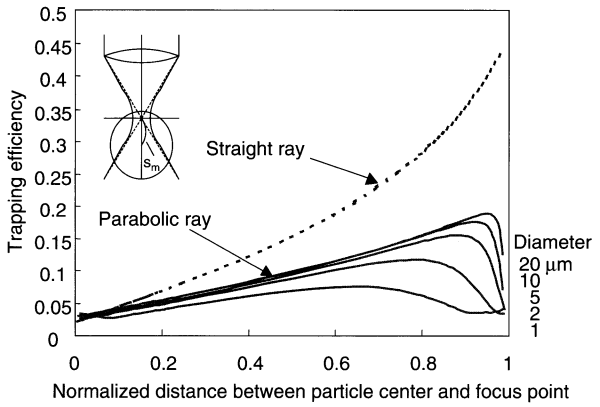

Fig. 3. Axial trapping efficiency dependence on normalized distance between sphere center and trapping position for polystyrene microsphere suspended in water by converging ray approximations of straight line and parabolic line with beam waist ω.

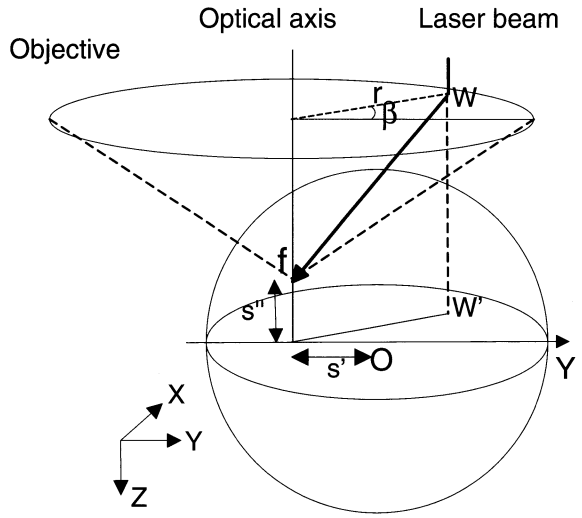

Fig. 4. Analysis model for calculating off-axis trapping efficiency of polystyrene microsphere. The laser focus is located s' from the center of the microsphere on the axis perpendicular to the optical axis, and s'' on the axis parallel to the optical axis.

trapping efficiencies are analyzed for an arbitrary focal position in the microsphere. Figure 5(a) shows the sectional view of the off-axis trapping for analysis; a ray enters at W(r, β) on the objective lens, refracts at V on the sphere surface, focuses at f (s' on the y-axis and s'' on the z-axis), and makes an angle γ with the xy-plane at P. Here, the plane WVfPBW′ is perpendicular to the xy-plane. The plane OVP makes an angle γ' with the xy-plane at P, where O is the center of the sphere. Figure 5(b) shows a developed view of the tetrahedron shown in (a).

The following relationships are realized by the geometry:

$$\tan\beta' = \frac{s'\sin\beta}{s'\cos\beta + \dfrac{s''}{\tan\alpha}} \tag{5}$$

$$\cos\gamma' = \cos\alpha\cos\beta' \tag{6}$$

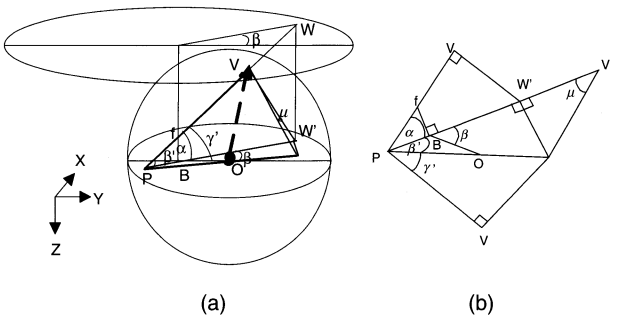

Fig. 5. (a) Geometry for calculating off-axis trapping efficiency of polystyrene microsphere, and (b) developed view of the tetrahedron in (a).

$$d = \frac{s''}{\tan\alpha}\cos\beta' + s'\cos(\beta - \beta') \tag{7}$$

$$R\sin\theta_1 = d\sin\gamma' \tag{8}$$

$$\cos\mu = \frac{\tan\alpha}{\tan\gamma'} \tag{9}$$

We can obtain angle β' from eq. (5), γ' from eq. (6), length d (= OP) from eq. (7), angle of incidence θ_1 from eq. (8) with sphere radius $R = 1$, and angle μ made by the W′VP plane with the OVP plane from eq. (9).

First, total trapping efficiency Q_t is calculated using the same steps described above for the incident rays in the first quadrant of the objective lens. To integrate the contribution of all rays within the convergent angle, the y-components of the scattering trapping efficiency and gradient trapping efficiency and the z-components of those for each ray are calculated, and then summed to obtain $Q^y_{s1}(s', s'')$, $Q^y_{g1}(s', s'')$, $Q^z_{s1}(s', s'')$, and $Q^z_{g1}(s', s'')$. Then, the total trapping efficiency in the first quadrant $Q_{t1}(s', s'')$ at the focal point (s', s'') is obtained as $Q_{t1} = \sqrt{Q^2_{s1} + Q^2_{g1}}$. We proceed with the rays incident in the second, third, and fourth quadrants on the objective lens. The four total trapping efficiencies $Q_{t1}(s', s'')$, $Q_{t2}(s', s'')$, $Q_{t3}(s', s'')$, $Q_{t4}(s', s'')$ are summed to get the final total trapping efficiency $Q_t(s', s'')$.

In the final step, we obtain the overall $Q^y_s(s', s'')$, $Q^y_g(s', s'')$, $Q^y_t(s', s'')$ shown in Fig. 6, $Q^z_s(s', s'')$, $Q^z_g(s', s'')$, $Q^z_t(s', s'')$ shown in Fig. 7, and finally the total trapping efficiency $Q_t(s', s'')$ shown in Fig. 8 at the trap position (s', s''). Figure 8 shows the magnitude and direction of Q_t at an arbitrary trap position for a polystyrene microsphere in the yz-plane. The magnitude of Q_t increases in all directions as the radius increases and is maximized close to the edge surface of the microsphere. The dotted line EE′ in Fig. 8 represents the locations for which the z-component of the trapping force is zero, i.e., the net force is purely transversal.

3. Experimental Analysis

3.1 Axial trapping

To measure the minimum axial trapping power $P^{\min,ax}_{exp}$, first, polystyrene spheres are dispersed in water and trapped by a circularly polarized laser beam converged by a 1.25-NA objective lens. Second, the power of the trapping beam is decreased until the microsphere is observed to fall out of the

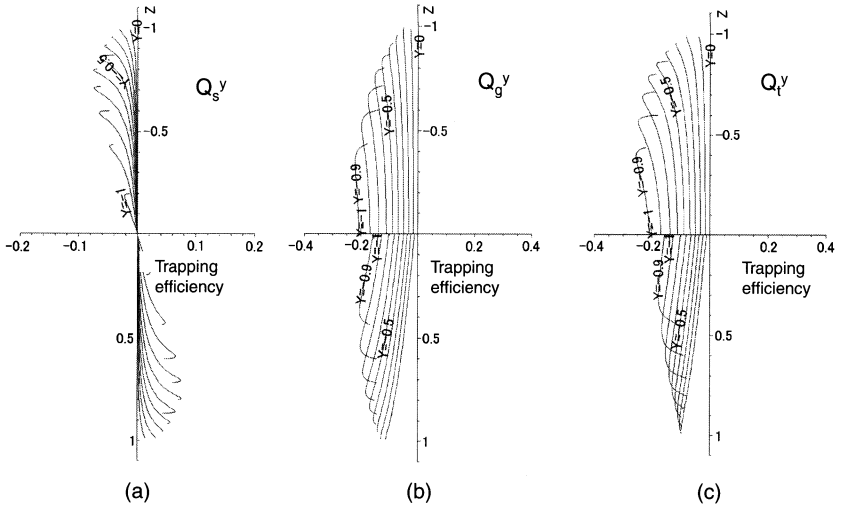

Fig. 6. Y-components of scattering trapping efficiency $Q_s^y(s', s'')$, gradient trapping efficiency $Q_g^y(s', s'')$, and total trapping efficiency $Q_t^y(s', s'')$.

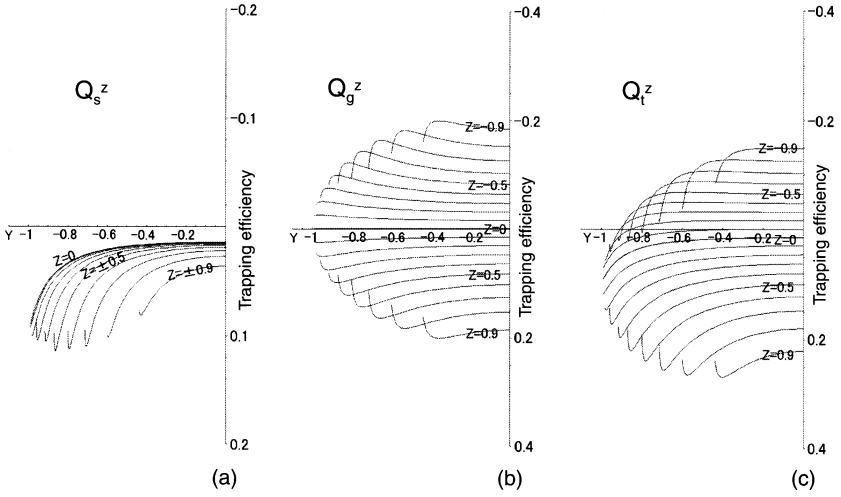

Fig. 7. Z-components of scattering trapping efficiency $Q_s^z(s', s'')$, gradient trapping efficiency $Q_g^z(s', s'')$, and total trapping efficiency $Q_t^z(s', s'')$.

trap. This $P_{\text{exp}}^{\text{min,ax}}$ is taken to be the difference between the gravitational and buoyant forces.

Figure 9 shows the dependence of the measured $P_{\text{exp}}^{\text{min,ax}}$ on sphere diameter d at $T = 10\,\mu\text{m}$ for the polystyrene spheres, where T is the distance of the laser focal point from the coverslip. $P_{\text{exp}}^{\text{min,ax}}$ with the upward-directed laser beam is less than that with the downward-directed laser beam because the scattering force is added to the gradient force to trap the particle with the upward-directed beam.

The theoretical minimum axial trapping power $P_{\text{theo}}^{\text{min,ax}}$ is shown by the solid line (upward directed) and the dotted line (downward directed) from eq. (10),[15] in which the trapping force is balanced by gravity, buoyancy, and Brownian movement (the theoretical trapping power is calculated using the expression $P_{\text{theo}}^{\text{ax}} = F_{\text{theo}}^{\text{ax}} c / n_1 Q_t^{\text{ax}}$):

$$P_{\text{theo}}^{\text{min,ax}} = \frac{c\left[\frac{\pi}{6}(\rho_s - \rho_m)d^3 g + \frac{2kT}{d}\right]}{n_1 Q_t^{\text{max,ax}}}, \qquad (10)$$

where ρ_s and ρ_m are the densities of the microspheres and suspending medium, respectively; d is the diameter of the spheres, c is the speed of light in vaccum, g is the gravitational acceleration, and kT is the thermal energy. A discrepancy between the predicted and the measured forces is observed.

Figure 10 shows the minimum axial trapping power $P_{\text{exp}}^{\text{min,ax}}$ (upward directed) for polystyrene microspheres comparing the experimental measurements with the predicted results for a straight-ray model (dotted line) and a parabolic-ray model (solid line). It is seen from the figure that $P_{\text{theo}}^{\text{min,ax}}$ largely increases for the parabolic-ray model and is close to the experimental results. This is because the actual focused trapping laser beam has a beam waist (parabolic ray) and the individual ray enters almost vertically to the sphere surface, as shown in the sketch in Fig. 3, leading to a reduced trapping efficiency (increased laser power).

3.2 *Transverse trapping*

Next, the minimum transverse trapping power $P_{\text{exp}}^{\text{min,trans}}$ was measured as the minimum power necessary to trap a particle moving at a constant velocity v in water. The theoretical transverse trapping power $P_{\text{theo}}^{\text{min,trans}}$ can be expressed as eq. (11)[15] by considering the viscous drag force and the maximum total trapping efficiency $Q_t^{\text{max,trans}}$ (= 0.406) in Fig. 1(b).

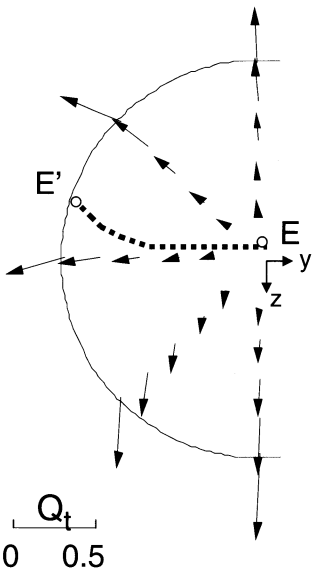

Fig. 8. Magnitude and direction of total trapping efficiency $Q_t(s', s'')$ for polystyrene microsphere at focal position (s', s'') in yz-plane. A circularly polarized laser beam uniformly fills the objective aperture of NA = 1.25.

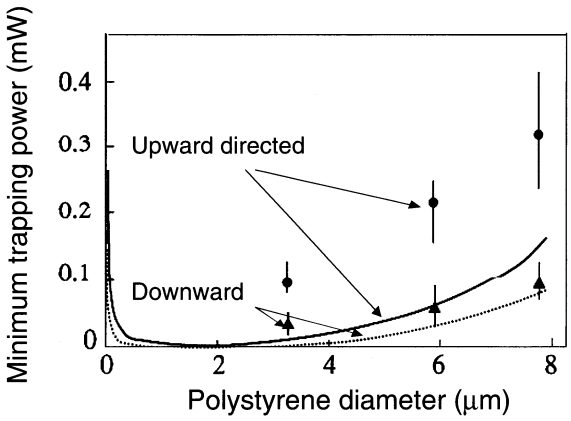

Fig. 9. Dependence of minimum axial trapping power on diameter of polystyrene microspheres.

$$P_{\text{theo}}^{\text{min,trans}} = \frac{3\pi\mu dvc\left[1 + \dfrac{9d}{32}\left(\dfrac{1}{T} - \dfrac{1}{H-T}\right)\right]}{n_1 Q_t^{\text{max,trans}}} \quad (11)$$

Here, μ and n_1 are the viscosity and the index of refraction of the suspending medium (water), respectively; T is the trapping depth, and H is the height of the specimen chamber (150 μm).

A comparison is made for the transverse trapping power. Figure 11 shows the dependence of $P_{\text{exp}}^{\text{min,trans}}$ on sphere velocity for $d = 10\,\mu$m polystyrene spheres (small gravity). $P_{\text{exp}}^{\text{min,trans}}$ increases as sphere velocity increases and the experimental values are in fairly good agreement with the theoretical ones in which the trapping position moves along the transverse centerline in the sphere.

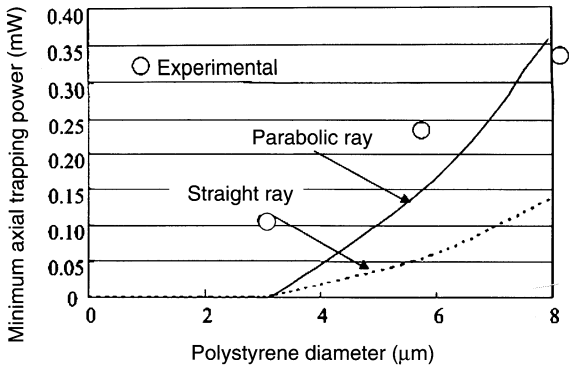

Fig. 10. Minimum axial trapping power for polystyrene microsphere, comparing experimental measurement with predicted results for straight-ray (ray optics) and parabolic-ray (beam waist) models.

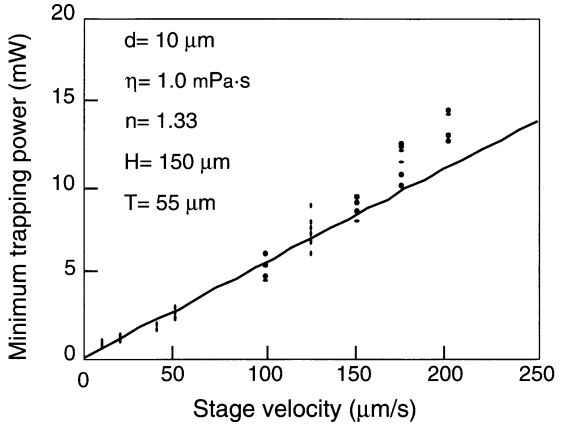

Fig. 11. Dependence of minimum transverse trapping power on velocity for $d = 10\,\mu$m for polystyrene microspheres.

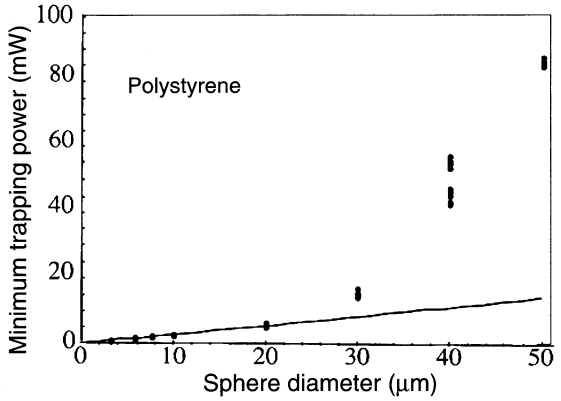

Fig. 12. Dependence of minimum axial trapping power on diameter for polystyrene microspheres. The discrepancy between theoretical and experimental results comes from the fact that the trapping position moves upward due to the gravitational force, which decreases Q_t.

Figure 12 shows the dependence of $P_{\text{exp}}^{\text{min,trans}}$ on sphere size (diameter) for polystyrene particles with a downward-directed beam. $P_{\text{exp}}^{\text{min,trans}}$ significantly increases as d increases due to the Stokes drag force increase. The discrepancies

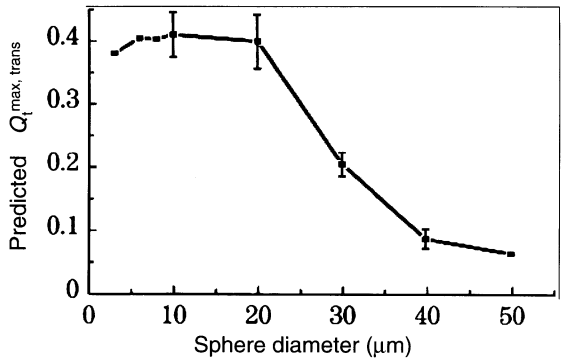

Fig. 13. Dependence of predicted $Q_t^{max,trans}$ on sphere diameter for polystyrene microsphere, which is derived from experimental data of Fig. 12. $Q_t^{max,trans}$ decreases as diameter increases.

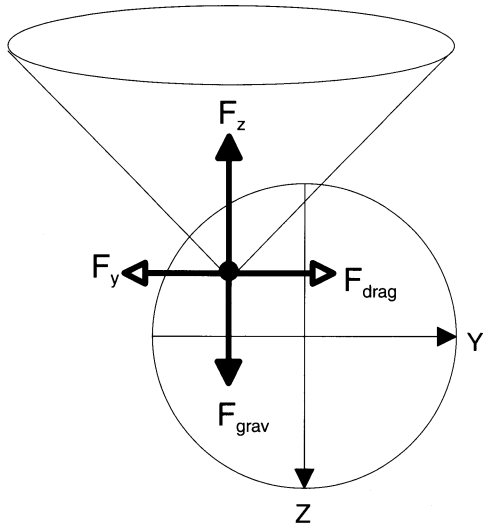

Fig. 14. Balances between y-component trapping force and viscous drag force, and between z-component trapping force and gravitational force, for microsphere moving at a constant velocity v in water. F_y $(= Q_{t\text{-}y}^{max} n_1 P_{min}/c) = 3\pi\mu dvc\{1 + (9d/32)[(1/T) - [1/(H-T)]]\}$. F_z $(= Q_{t\text{-}z}^{max} n_1 P_{min}/c) = (\pi/6)(\rho_s - \rho_m)d^3 g + 2kT/d$.

between the theory and experiment for the trapping forces at $d > 30\,\mu m$ are due to the fact that the trapping position moves to upward from the transverse centerline in the sphere, which decreases Q_t, because the gravitational force increases for such large spheres.

4. Trajectory of Trapping Position in Microspheres

The experimental maximum transverse total trapping efficiency $Q_t^{max,trans}$ can be obtained from Fig. 12 using eq. (11), as shown in Fig. 13, resulting in the fact that $Q_t^{max,trans}$ decreases as the polystyrene diameter increases. The reasons are as follows.

As the trapping power decreases, the microsphere moving at the constant velocity of v in water escapes the trap, either because the viscous drag force becomes greater than the transverse trapping force $F_{t\text{-}y}^{min}$, or because the difference between the gravitational force and the buoyancy becomes

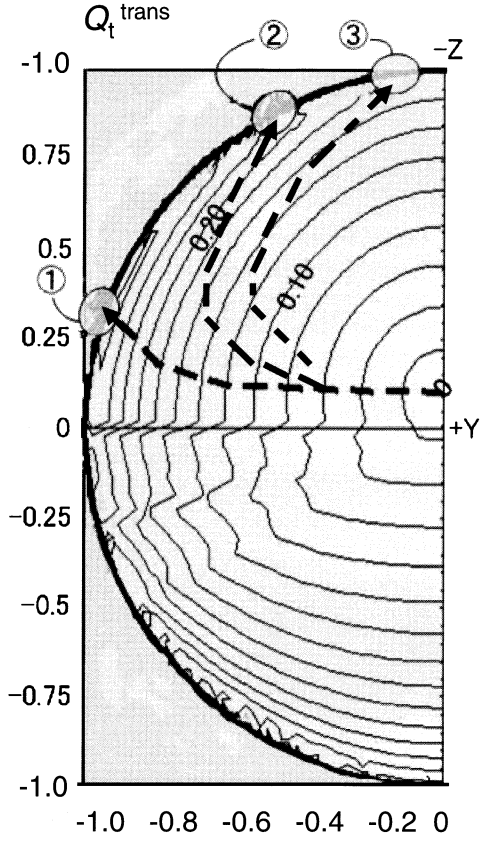

Fig. 15. Contour lines for total trapping efficiency Q_t of polystyrene microspheres; expected trajectory of trapping (focal) position in polystyrene is shown by location 1 for a diameter less than 20 μm; location 2 for the diameter of 30 μm; and location 3 for a diameter greater than 40 μm.

greater than the axial trapping force $F_{t\text{-}z}^{min}$. Figure 14 shows the equilibrium conditions for (1) viscous drag force (y-component) and (2) gravitational force (z-component) for the microsphere moving at the velocity of v.

On the other hand, the contour lines of the total trapping efficiency $Q_t = \sqrt{(Q_t^y)^2 + (Q_t^z)^2}$ are obtained using Q_t^y in Fig. 6(c) and Q_t^z in Fig. 7(c), as shown in Fig. 15. It is found that Q_t increases as the focus moves from the center to the outer part (edge surface) of the microsphere. The contour lines have a pitch of 0.02.

In the figure, location 1 $(-0.95, -0.30)$ has a maximum trapping efficiency of 0.40, which is in agreement with the experimental transverse trapping efficiency $Q_t^{max,trans}$ $(Q_{t\text{-}y}^{max})$ for diameters less than 20 μm, resulting in ignoring of the effect of gravity. The dotted line shows the trajectory of the trapping position for this case, i.e., the z-component of the trapping force equals zero, as described in §2.3. The transverse trapping force balances the drag force. Location 2 $(-0.48, -0.87)$ has a maximum trapping efficiency of 0.20, in agreement with $Q_t^{max,trans}$ for a diameter of 30 μm, which means that the equilibrium position moves along the edge surface to location 2 due to gravity, but escapes the trap of the drag force becoming greater than the transverse trapping force F_y. Nevertheless, location 3 $(-0.17, -0.99)$ has a

maximum trapping efficiency of 0.17, which does not agree with $Q_t^{max,trans}$ for a diameter of 40 to 50 μm. This means that the microsphere escapes when the gravitation force becomes greater than the axial trapping force F_z, i.e., it escapes the trap as a result of the gravitational force (z-component), rather than the viscous drag force (y-component).

As a result, when the trapping power decreases, the equilibrium position moves along the dotted lines (the expected trajectories of the trapping position in the polystyrene) to location 1 for a diameter less than 20 μm; location 2 for the diameter of 30 μm; and location 3 for a diameter greater than 40 μm, as shown in Fig. 15.

5. Conclusions

Basic optical trapping characteristics for polystyrene microspheres of different diameters are analyzed and comparisons between theoretical and experimental findings are given. In theoretical analysis, not only the conventional straight-ray approximation but also parabolic-ray approximation is used to calculate trapping forces. In experimental analysis, particles are trapped with both upward- and downward-directed YAG laser beams, and minimum laser powers for both axially and transversally trapped particles are measured.

Trapping power discrepancies between theory and experiment come from both axial and transverse trappings. The former discrepancy is resolved by taking into account the parabolic-ray model with a beam waist instead of the straight-ray model, and the latter discrepancy by considering the trapping efficiency decrease due to the trapping (focal) position displacement by gravity.

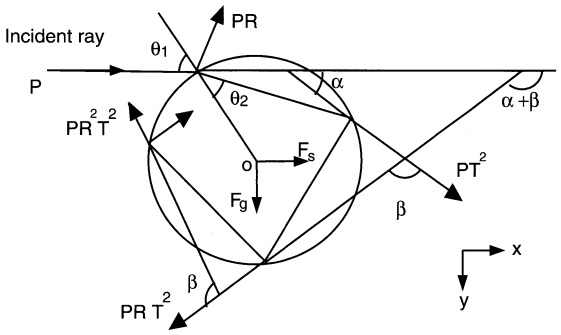

Fig. A·1. Optical pressure force on microsphere exerted by single incident ray.[14)]

Appendix

Consider a ray of power P incident to a microsphere at angle θ_1. Figure A·1 shows the geometry for this model and trapping force F is calculated in accordance with Ashkin.[14)] The respective expressions of the net optical pressure by the emerging rays in the direction parallel (F_s: scattering force) and perpendicular (F_g: gradient force) to the incident ray can be expressed as

$$F_s = \left\{1 + R\cos 2\theta_1 - \frac{T^2[\cos 2(\theta_1 - \theta_2) + R\cos 2\theta_1]}{1 + R^2 + 2R\cos 2\theta_2}\right\}\frac{n_1 P}{c} = Q_s\frac{n_1 P}{c} \quad \text{(A·1)}$$

$$F_g = \left\{R\sin 2\theta_1 - \frac{T^2[\sin 2(\theta_1 - \theta_2) + R\sin 2\theta_1]}{1 + R^2 + 2R\cos 2\theta_2}\right\}\frac{n_1 P}{c} = Q_g\frac{n_1 P}{c} \quad \text{(A·2)}$$

where θ_1 is the angle of incidence, θ_2 is the angle of refraction, T and R are the Fresnel transmission and reflection coefficients, and Q_s and Q_g are the scattering and gradient trapping efficiencies, respectively. As a result, total Q_t and total F_t are

$$Q_t = \sqrt{Q_s^2 + Q_g^2}, \quad \text{(A·3)}$$

$$F_t = \sqrt{F_s^2 + F_g^2} = Q_t\frac{n_1 P}{c}. \quad \text{(A·4)}$$

References

1) A. Ashkin, J. M. Dziedzic, J. E. Bjorkholm and S. Chu: Opt. Lett. **11** (1986) 288.
2) H. Misawa, K. Sasaki, M. Koshioka, N. Kitamura and H. Masuhara: Appl. Phys. Lett. **60** (1992) 310.
3) M. E. J. Friese, T. A. Nieminen, N. R. Heckenberg and H. Rubinsztein-Dunlop: Nature **394** (1998) 348.
4) E. Higurashi, R. Sawada and T. Ito: Phy. Rev. E **59** (1999) 3676.
5) M. J. Padgett, J. Leach, G. Sinclair, J. Courtial, E. Yao, G. Gibson, P. Jordan, J. Cooper and J. Laczik: Proc SPIE **5514** (2004) 371.
6) S. Juodkazis, N. Mukai, R. Wakaki, A. Yamaguchi, S. Matuo and H. Misawa: Nature **408** (2000) 178.
7) E. Higurashi, H. Ukita, H. Tanaka and O. Ohguchi: Appl. Phys. Lett. **64** (1994) 2209.
8) H. Ukita and K. Nagatomi: Appl. Opt. **42** (2003) 2708.
9) K. Svobada, C. F. Schmidt, B. J. Schnap and S. M. Block: Nature **365** (1993) 721.
10) A. Ishijima, H. Kojima, T. Funatsu, M. Tokunaga, H. Higuchi, H. Tanaka and T. Yanagida: Cell **92** (1998) 161.
11) S. Ito, Y. Yoshikawa and H. Masuhara: Appl. Phys. Lett. **78** (2001) 2566.
12) A. Simon and A. Libchaber: Phys. Rev. Lett. **68** (1992) 3375.
13) M. Miwa, H. Misawa, H. Araki and T. Yoshimura: Proc. Int. Symp. Microsystems, Intelligent Materials and Robots, 1995, p. 67.
14) A. Ashkin: Biophys. J. **61** (1992) 569.
15) H. Felgner, O. Muller and M. Schliwa: Appl. Opt. **34** (1995) 977.
16) H. Ukita and T. Saitoh: IEEE Lasers and Electro-Optics Society Annual Meeting (LEOS '99), 1999, p. 169.